HHS Public Access

Author manuscript

Sci Signal. Author manuscript; available in PMC 2015 November 25.

Published in final edited form as:

Sci Signal. ; 7(340): ra81. doi:10.1126/scisignal.2005334.

Semaphorin 3A activates the guanosine triphosphatase Rab5 to promote growth cone collapse and organize callosal axon projections

Kong-Yan Wu[1], **Miao He**[1], **Qiong-Qiong Hou**[1], **Ai-Li Sheng**[1], **Lei Yuan**[1], **Fei Liu**[1], **Wen-Wen Liu**[2], **Guangpu Li**[3], **Xing-Yu Jiang**[2], and **Zhen-Ge Luo**[1,*]

[1]Institute of Neuroscience, State Key Laboratory of Neuroscience, Shanghai Institutes for Biological Sciences, Chinese Academy of Sciences, 320 Yue Yang Road, Shanghai 200031, China

[2]Chinese Academy of Sciences Key Laboratory for Biological Effects of Nanomaterials and Nanosafety, National Center for Nanoscience and Technology, 11 Beiyitiao, Zhong Guan Cun, Beijing 100190, China

[3]Department of Biochemistry and Molecular Biology, University of Oklahoma Health Sciences Center, Oklahoma City, OK 73104, USA

Abstract

Axon guidance (pathfinding) wires the brain during development and is regulated by various attractive and repulsive cues. Semaphorin 3A (Sema3A) is a repulsive cue, inducing the collapse of axon growth cones. In the mammalian forebrain, the corpus callosum is the major commissure that transmits information flow between the two hemispheres, and contralateral axons assemble into well-defined tracts. We found that the patterning of callosal axon projections in rodent layer II and III (L2/3) cortical neurons in response to Sema3A was mediated by the activation of Rab5, a small guanosine triphosphatase (GTPase) that mediates endocytosis, through the membrane fusion protein Rabaptin-5 and the Rab5 guanine nucleotide exchange factor (GEF) Rabex-5. Rabaptin-5 bound directly to Plexin-A1 in the Sema3A receptor complex [an obligate heterodimer formed by

*Corresponding author. zgluo@ion.ac.cn.

SUPPLEMENTARY MATERIALS

www.sciencesignaling.org/cgi/content/full/7/340/ra81/DC1

Fig. S1. Quantification of protein interactions.
Fig. S2. Rab5 distribution in brain slices and cultured cortical neurons.
Fig. S3. Regulation of Rab5 activity by other guidance cues.
Fig. S4. Efficacy and specificity of the GST-R5BD probe in cultured L2/3 neurons.
Fig. S5. Specificity of Rab5 siRNA and role of Rab10 in axonal growth cones.
Fig. S6. Recognition of cortical regions after electroporation.
Fig. S7. Role of Rab5 isoforms in cortical neuron migration.
Fig. S8. Role of Rab5b in cortical neuron migration.
Fig. S9. Effects of Rab5 manipulations on the differentiation of cortical neural progenitors.

Author contributions: K.-Y.W. and Z.-G.L. designed the research; K.-Y.W. performed most of the research; M.H., Q.-Q.H., A.-L.S., and L.Y. generated specific constructs or assisted with Western blot analysis; F.L. helped with in utero electroporation; W.-W.L. and X.-Y.J. provided PDMS molds for microfluidic culture device and stripe assays; G.L. provided Rab5 and GST-R5BD plasmids; K.-Y.W. and Z.-G.L. analyzed the data; and K.-Y.W. and Z.-G.L. wrote the paper.

Competing interests: The authors declare that they have no competing interests.

Data and materials availability: A material transfer agreement is required for expression constructs of Rab5 and GST-R5BD.

Plexin-A1 and neuropilin 1 (NP1)]; Sema3A enhanced this interaction in cultured neurons. Rabaptin-5 bridged the interaction between Rab5 and Plexin-A1. Sema3A stimulated endocytosis from the cell surface of callosal axon growth cones. In utero electroporation to reduce Rab5 or Rabaptin-5 impaired axon fasciculation or caused mistargeting of L2/3 callosal projections in rats. Over-expression of Rabaptin-5 or Rab5 rescued the defective callosal axon fasciculation or mistargeting of callosal axons caused by the loss of Sema3A–Plexin-A1 signaling in rats expressing dominant-negative Plexin-A1 or in NP1-deficient mice. Thus, our findings suggest that Rab5, its effector Rabaptin-5, and its regulator Rabex-5 mediate Sema3A-induced axon guidance during brain development.

INTRODUCTION

A number of guidance cues are involved in axon pathfinding or fasciculation (*1*, *2*). Semaphorin 3A (Sema3A), originally designated as SemaD, SemaIII, or collapsin-1, induces growth cone collapse and axon repulsion in culture (*3*–*5*) and is one of the class III secreted semaphorins that affect axon guidance (*6*, *7*), neuronal migration (*8*), axon-dendrite polarity (*9*–*11*), and synapse formation (*12*, *13*). Genetic ablation of *Sema3A* in mice causes abnormal orientation of neuronal processes of the pyramidal neurons in the cerebral cortex and inappropriate projection of sensory afferents in the spinal cord (*14*, *15*) and several abnormalities in peripheral nerve fasciculation (*16*).

The role of Sema3A in growth cone guidance is believed to be mediated through a receptor complex comprising neuropilin 1 (NP1) as the ligand-binding subunit and Plexin-A1 as the signal-transducing subunit (*17*–*20*). *NP1* mutant mice display malformation of the forebrain commissures (*21*). Several intracellular molecules are involved in Sema3A-induced growth cone collapse or axonal repulsion (*22*–*25*). Most of these molecules contribute to Sema3A-induced repulsion through modulating cytoskeleton dynamics, and growth cone collapse is accompanied by a reduction in the area of growth cone plasma membrane. Additionally, Sema3A induces receptor endocytosis during growth cone collapse (*26*), and asymmetric endocytosis mediates repulsive growth cone guidance (*27*).

The Rab family of small monomeric G proteins (heterotrimeric guanine nucleotide–binding proteins) plays critical roles in various membrane trafficking events, including vesicle formation, transportation, docking, and fusion in eukaryotic cells (*28*, *29*). Among more than 70 mammalian Rabs, three Rab5 isoforms (Rab5a, Rab5b, and Rab5c) function primarily within the endocytotic pathway (*30*), which mainly promotes homotypic early endosome fusion (*31*, *32*) and increases motility of endosomes (*33*) and the rate of endocytosis (*34*). Like other Rab proteins, Rab5 can be activated by guanine nucleotide exchange factors (GEFs), which trigger the exchange of guanosine diphosphate (GDP) for guanosine triphosphate (GTP) and are inactivated by guanosine triphosphatase (GTPase)–activating proteins (GAPs), which hydrolyze the bound GTP to GDP (*35*). In neurons, Rab5-mediated endocytosis occurs within both somatodendritic and axonal domains (*36*). Rab5-mediated internalization of synaptic α-amino-3-hydroxy-5-methyl-4-isoxazolepropionic acid (AMPA) receptors is associated with long-term depression (LTD) in hippocampal neurons (*37*). Rab5-mediated endocytosis is also involved in the axonal retrograde transport pathway (*38*),

as well as in the migration of newborn neurons in the neocortex by modulating surface abundance of the cell adhesion molecule N-cadherin (*39*). In addition, Rab5 activation inhibits neurite outgrowth in the rat pheochromocytoma cell line PC12 (*40*). Rabaptin-5, a direct effector of Rab5, specifically interacts with GTP-bound Rab5 and mediates membrane fusion during endocytosis (*41*).

In the mammalian forebrain, commissural axons derived from specific cellular layers are usually assembled into well-defined tracts. The corpus callosum composed of callosal axons mainly emanating from layers II/III cortical (L2/3) neurons is the major commissure that transmits information flow between two hemispheres (*42*, *43*). The present study aimed to explore the mechanism through which Sema3A controls patterning of callosal axons, and specifically investigated the role of Rab5 in mediating Sema3A signaling during callosal axon tract development.

RESULTS

Rabaptin-5 interacts with Plexin-A1

Binding of semaphorin to the neuropilinplexin holoreceptor complex triggers activation of intracellular signaling mediated by the cytoplasmic domain of plexin (*25*). To gain insights into the mechanisms of Sema3A–Plexin-A1 signaling, we used affinity purification and liquid chromatography with tandem mass spectrometry (LC-MS/MS) to identify proteins in neonatal rat upper-layer cortex homogenates that bound the cytoplasmic domain of Plexin-A1 (cytoPlexin-A1) fused with glutathione S-transferase (GST) (Fig. 1A). LC-MS/MS analysis identified Rabaptin-5 as hit. As a control, 14-3-3 family of phosphoserine-binding proteins, which antagonizes semaphorin-induced repulsion (*44*), was also in the list. Interaction between Plexin-A1 and Rabaptin-5 was further confirmed in immunoprecipitation and pull-down assays. Rabaptin-5 interacted with Plexin-A1 in homogenates from the rat upper cortex (Fig. 1B). GST–cytoPlexin-A1, but not GST alone, pulled down exogenous Rabaptin-5 expressed in human embryonic kidney (HEK) 293 cells (Fig. 1C). This interaction was direct, because GST–cytoPlexin-A1 pulled down affinity-purified hexahistidine (His6)–tagged Rabaptin-5 (Fig. 1D). The relationships among Rabaptin-5, Plexin-A1, and Rab5 were determined in HEK293 cells that were cotransfected with hemagglutinin (HA)–tagged cytoPlexin-A1 and Rab5, with or without Rabaptin-5. Rabaptin-5 interacted with Plexin-A1 and Rab5b simultaneously, suggesting the formation of the complex composed of Plexin-A1, Rabaptin-5, and Rab5 (Fig. 1E and Fig. S1A). More Rab5 were associated with Plexin-A1 in cells with ectopic Rabaptin-5 (Fig. 1F and Fig. S1B), indicating that Rabaptin-5 mediates the association between Rab5 and Plexin-A1.

Next, we determined the abundance of Rab5 during rat cortex development. We found that Rab5 was low at early developmental stages, increased from late embryonic stage (E17.5), peaked at around 2 to 3 weeks after birth, and declined thereafter (Fig. S2A). This time course is coincidental with the period for the development and refinement of the callosal projections (*43*). Examining regional distribution of Rab5 in the E17.5 rat brain, we found that Rab5 was present in the ventricular and subventricular zone, as well as in cortical plate (CP) layers II/III, which were marked by transcription factor special AT-rich sequence-binding protein 2 (Satb2) (Fig. S2B) (*45*, *46*). Rab5 abundance was greater in Satb2-positive

(Satb2$^+$) than in Satb2-negative (Satb2$^-$) neurons (Fig. S2, C and D). Indeed, nearly 70% of cultured cortical neurons isolated from upper layers, transfected with green fluorescent protein (GFP) to mark neuronal morphology, were positive for Satb2 (Fig. S2, E and F). Given that Sema3A receptors are distributed in the corpus callosum (*5*, *47*, *48*), we determined the responsiveness of L2/3 neurons to Sema3A stimulation. We found that shortly after Sema3A treatment (5 to 10 min), the association between Rabaptin-5 and Plexin-A1 was markedly increased (Fig. 1G and Fig. S1C). In line with this observation, a short treatment with Sema3A (5 min) increased the amount of Plexin-A1 that was colocalized with Rab5 in the axonal growth cones of L2/3 neurons before the appearance of growth cone collapse (Fig. 1, H and I). Thus, Sema3A enhances the recruitment of Rab5 to Plexin-A1 in callosal neurons, likely through Rabaptin-5.

Sema3A signaling activates Rab5

The formation of the Plexin-A1–Rabaptin-5–Rab5 complex may facilitate the activation of Rab5 by Sema3A. We determined Rab5 activity in L2/3 neurons treated with Sema3A for different time periods by a pull-down assay using a GST-fused Rab5 binding domain of Rabaptin-5, hereafter referred to as R5BD, which specifically recognizes the GTP-bound active form of Rab5 (Rab5-GTP) (*40*, *49*). We found that Sema3A treatment markedly increased the abundance of Rab5-GTP, which peaked 20 min after Sema3A treatment (Fig. 2, A and B). This activation was not observed in neurons treated with other guidance cues that regulate midline crossing, such as Netrin1, Slit2, or EphrinA2 (Fig. S3, A to C). Thus, Sema3A specifically activates Rab5 in cortical neurons. Next, we determined spatial activity of Rab5 in axonal growth cones with GST-R5BD as a probe, followed by staining with an antibody against GST. The amount of GST-R5BD was increased in axonal growth cones of L2/3 neurons that overexpressed wild-type or a constitutively active mutant (Q79L) of Rab5, whereas expression of the dominant-negative mutant (S34N) of Rab5 (dnRab5b) exhibited an opposite effect (Fig. S4, A and B). These results indicate the efficacy and specificity of the GST-R5BD probe in detecting the spatial activity of Rab5. Using this probe, we found that Sema3A treatment (5 min) markedly increased the abundance of Rab5-GTP in growth cones of cultured L2/3 neurons (Fig. 2, D and E). This increase was prevented in neurons transfected with small interfering RNA (siRNA) against Rabaptin-5 (Fig. 2, C to E) (*50*) or Rabex-5, a GEF for Rab5 (*51*). Thus, the Sema3A-induced activation of Rab5 requires Rabaptin-5 and Rabex-5. In line with this notion, Rabaptin-5 was associated with Rabex-5 in L2/3 neurons (Fig. 2F). The interaction between Rabaptin-5 and Plexin-A1 may initiate the formation of a signaling platform that facilitates Rab5 activation by Sema3A.

Given that the Plexin-A1–NP1 complexes form functional Sema3A receptors (*20*, *52*), we investigated the relationship between NP1 and Rab5 activity by analyzing the abundance of Rab5-GTP in *NP1* mutant mice. We restricted *NP1* deletion in dorsal telencephalic progenitors, by crossing *NP1*$^{floxed/floxed}$ (*NP1*$^{f/f}$) mice (*21*) with Emx1-Cre transgenic mice (*53*). We found that in the cortex and hippocampus of *NP1*$^{f/f}$; *Emx-Cre* mice, Rab5 activity was markedly decreased compared with control *NP1*$^{f/f}$ littermates (Fig. 2, G and H). Thus, NP1 is involved in Rab5 activation in the brain.

Rab5 mediates Sema3A-induced axonal growth cone collapse

Sema3A induces axonal growth cone collapse in various neuronal cell types, including sensory ganglion neurons and cortical and hippocampal neurons (*3, 54–56*). In agreement with this, we found that axons of Satb2$^+$ L2/3 neurons cultured for 3 DIV exhibited marked growth cone collapse after treatment with Sema3A, as reflected from increased percentage of collapsed growth cones (Fig. 3, C and D) and decreased growth cone area (Fig. 3, C and E). Growth cone volume was marked by GFP expressed by pSUPER plasmids transfected into cells. Next, we determined the role of Rab5 in Sema3A-induced growth cone collapse. Three selected siRNAs were effective in suppressing the abundance of Rab5b, in comparison to corresponding scrambled sequences (Fig. 3, A and B), but had no effects on the abundance of several other Rabs, including Rab7, Rab8, or Rab10 (Fig. S5, A to C). When transfected with pSUPER plasmids encoding one of two Rab5b siRNAs, the effect of Sema3A in inducing the axonal growth cone collapse was markedly attenuated (Fig. 3, C to E). Transfection with Rab5b siRNA itself had no effect on mock-treated axonal growth cones (Fig. 3, C to E). Thus, Rab5b is essential for Sema3A-induced axonal growth cone collapse of cortical callosal neurons. We predicted that overexpression of cytoPlexin-A1 may act as dominant-negative form through the competition with endogenous Plexin-A1 for intracellular binding proteins, such as Rabaptin-5. As expected, overexpression of cytoPlexin-A1 prevented growth cone collapse induced by Sema3A (Fig. 3, C to E).

To determine the role of Rab5 in axonal growth cone dynamics directly, L2/3 neurons were transfected with plasmids encoding Rab5b or Rabaptin-5 and analyzed for growth cone changes (Fig. 3F). We found that the increased Rab5b or Rabaptin-5 caused a reduction in growth cone area and an increase in the percentage of axons without apparent growth cones (Fig. 3, G and H). As a control, forced expression of Rab10 had no effect on the morphology of L2/3 axonal growth cones (Fig. S5, D to F). These results support the conclusion that Rab5 activation leads to collapse of axonal growth cones.

Sema3A induces endocytosis from the plasma membrane in a Rab5-dependent manner

Sema3A-induced growth cone collapse is associated with reduction in growth cone surface area (*57, 58*) and enhanced receptor endocytosis (*26*). However, the underlying molecular mechanism is unclear. The activation of Rab5 by Sema3A prompted us to determine the involvement of Rab5 in Sema3A-induced membrane endocytosis. First, we used dextran conjugated to Alexa Fluor 555 (Alexa-dextran) to label endocytic vacuoles. Isolated neurons were transfected with GFP plasmid and then incubated with Alexadextran in the presence or absence of Sema3A. We found that Sema3A treatment markedly increased dextran uptake at the axonal growth cone (Fig. 4, A and B), indicating increased endocytosis. This effect was attenuated in neurons transfected with siRab5b or cytoPlexin-A1 (Fig. 4, A and B), suggesting a critical role of Rab5b and Plexin-A1 signaling in Sema3A-induced endocytosis during growth cone collapse. Next, the neuronal plasma membrane was labeled with a lipophilic styryl compound FM4-64, which can insert into the outer leaflet of the surface membrane and thus has been used to mark plasma membrane endocytic vesicles (*59*). Similar to the result with dextran, Sema3A treatment increased endocytosis of FM4-64, in a manner dependent on Rab5b (Fig. 4, C and D). Thus, Rab5 plays an important role in Sema3A-induced membrane endocytosis.

Sema3A restrains axonal growth through Rab5

Induction of axonal growth cone collapse and membrane endocytosis may impair axonal growth and consequently prevent the projection of axons to surrounding regions containing repulsive cues, such as Sema3A. In addition to the CP, Sema3A is also distributed in regions encompassing the callosal axons in E17.5 rat brain tissue (Fig. 5A). In particular, Sema3A signals were detected near the midline corresponding to regions containing the indusium griseum glia and the subcallosal sling (Fig. 5A), both of which are considered sources of guidepost cues regulating midline crossing of callosal axons (*60, 61*). We hypothesized that Sema3A might act as a "surround repulsion" cue that constrains the defasciculation of callosal axon bundles. To test this hypothesis, we took advantage of the stripe assay to generate Sema3A boundaries in vitro (*62*). L2/3 neurons were transfected with either scrambled or Rab5b siRNA, and then plated on substrates with either Sema3A or control stripes of proteins. We noted that about half of control cells extended axons strictly restrained between Sema3A stripes, whereas the percentage of cells with this behavior was much lower when cultured on substrate with control stripes (Fig. 5, B and C). The constraint role of Sema3A boundary was not effective for neurons transfected with siRab5b (Fig. 5, B and C). These results suggest that Rab5 is required for Sema3A repulsion of callosal axons.

Considering the enriched distribution of Sema3A receptors in callosal axons, we determined the responsiveness of L2/3 axons to locally applied Sema3A in a microfluidic chamber system (Fig. 5D) (*63*). The presence of Sema3A provided an avoidance environment in the distal compartment, which prohibited the entrance of L2/3 axons (Fig. 5E). The effect of Sema3A was further evident in the reduced percentage and length of axons in axon compartments in the presence of Sema3A (Fig. 5, F and G). However, when neurons were transfected with siRab5b, the inhibitory effect of Sema3A was completely prevented (Fig. 5, E to G). These results suggest that Sema3A inhibits axon extension through Rab5 localized in axonal growth cones.

Rab5 is essential for fasciculation of cortical callosal axons

Growth cone collapse or the repellent activity of Sema3A is believed to play an important role in driving axon trajectories into fascicles (*7*). Indeed, defasciculation of periphery or central nervous system (CNS) axons has been observed in mutant mice with genetic ablation of *Sema3A* or its receptor *NP1* (*16, 21, 64, 65*). Given that Rab5 was activated by Sema3A and was involved in Sema3A-induced growth cone collapse, we determined the role of Rab5 in cortical callosal axon fasciculation. Because L2/3 neurons are born around E15.5 to E17.5 (*43, 66*), we manipulated the activity or abundance of Rab5 in a subpopulation of rat progenitors in the ventricular zone at E15.5 by using in utero electroporation. At different postnatal stages, axon projections of the S1 (primary somatosensory cortex) and S2 (secondary somatosensory cortex) were analyzed (Fig. S6, A to D). In the control group at P7, callosal axons were well organized into fascicles during and after crossing the midline (Fig. 6A). However, with the expression of dnRab5b, callosal axons exhibited abnormal defasciculation in these contralateral trajectories (Fig. 6A). In contrast to dnRab5b, overexpression of wild-type Rab5b decreased the relative width of callosal axon tracts (Fig. 6A). Similar to dnRab5b, in utero electroporation with either siRab5b or combination of constructs encoding siRNAs against all three Rab5 isoforms—Rab5a, Rab5b, and Rab5c

(Fig. 3, A and B, and Fig. S7, A to C)—induced the defasciculation of callosal axons (Fig. 6B). The extent of defasciculation was reflected from increased width of axon tracts relative to that of the white matter during and immediately after crossing the midline (Fig. 6, C to F). In many cases, callosal axons in siRab5b animals deviated from the main bundle and even invaded the ventral parenchyma underneath the corpus callosum (Fig. 6G). These results suggest that Rab5 activity controls callosal axon fasciculation.

A recent study has shown that several Rabs, including Rab5, are involved in multiple phases of neuronal migration through distinct endocytic pathways (*39*). However, the defasciculation defects were unlikely caused by the impairment in neuronal migration, because although either increase or decrease of Rab5 abundance caused a delay in the migration of newborn neurons to the CP at P0 (figs. S7, D and F, and S8, A and B), these phenomena were not seen in P3 animals (figs. S7, E and G, and S8, C and D). We also determined the effects of Rab5 manipulations on the cell fate determination of newborn neurons. We found that increase, decrease, or inhibition of Rab5 had no effect on the differentiation of cortical neuronal pre-cursors, as evidenced by the similar percentage of $Satb2^{+}$ post-mitotic upper-layer neurons (Fig. S9, A and B). Together, Rab5 plays a pivotal role in organizing the callosal axon bundles without affecting cell fate.

Rabaptin-5 and Plexin-A1 are involved in callosal axon fasciculation

Given that Rabaptin-5 mediates Sema3A–Plexin-A1 signaling for Rab5 activation, we next investigated the role of Rabaptin-5 in callosal axon fasciculation. Similar to the effect of siRab5 or dnRab5, electroporation with Rabaptin-5 siRNA also increased the relative width of callosal axon tracts, whereas overexpression of Rabaptin-5 decreased the relative width (Fig. 7, A to F). These results suggest that appropriate Rabaptin-5 abundance is critical for the maintenance of tight callosal axon bundles.

Next, we examined the role of Sema3–Plexin-A1 signaling in callosal axon fasciculation and the relationship with Rabaptin-5 and Rab5 in vivo. For this purpose, we electroporated E15.5 rat cortical progenitors with cytoPlexin-A1, which had been shown to be a dominant-negative form for Sema3A-induced growth cone collapse (Fig. 3, C to E) and membrane endocytosis (Fig. 4, A and B). As expected, forced expression of cytoPlexin-A1 caused defasciculation of callosal axon bundles, as reflected from the increased width of axon tracts (Fig. 7, B, E, and F); this phenomenon was similar with that which resulted from the loss of function of Rab5 or Rabaptin-5. Notably, the axonal defasciculation caused by cytoPlexin-A1 expression was prevented by cotransfection with Rabaptin-5 (Fig. 7, B, E, and F). A possible interpretation is that overexpressed Rabaptin-5 may scavenge the dominant-negative effect of cytoPlexin-A1 and thus enable the activation of Rab5 that controls axon fasciculation. Thus, Plexin-A1 signaling participates in constraining callosal axon bundles, probably through the Rabaptin-5–Rab5 system.

Rab5 and NP1 are important for proper patterns of callosal axon fasciculation

Having shown that the Rab5 activity is reduced in the *NP1*$^{f/f}$; *Emx1-Cre* mice brains (Fig. 2, G and H), we decided to determine patterns of callosal axon fasciculation in mice with NP1 knockout specifically in the S1/S2 regions, without or with Rab5 overexpression. For this

purpose, E15.5 *NP1*$^{f/f}$ mice were electroporated with Cre expression plasmid (ubiqutin-Cre-2A-GFP) or GFP, without or with Rab5b (Fig. 8A). We found that callosal axon defasciculation was observed in Cre-electroporated *NP1*$^{f/f}$ mice, and this defect was completely rescued by Rab5b expression (Fig. 8, A to C). This result indicates again the involvement of Rab5, which acts downstream of the Sema3A signaling, in the bundling of callosal axons.

Rab5 and NP1 determine precise callosal contralateral axon projections

A recent study showed that Sema3A-NP1 signaling is critical for the topographic ordering of cortical axons within the corpus callosum, which determines homotopic contralateral projections (*48*). The involvement of Rab5-mediated endocytosis in Sema3A signaling prompted us to determine the role of Rab5 in contralateral axon projections postnatally. We expressed GFP either alone or together with dnRab5b or wild-type Rab5b in L2/3 neurons of S1/S2 by in utero electroporation in E15.5 embryos. At P14, electroporated mouse brains were sectioned coronally and examined for callosal axon projections. Consistent with previous studies (*43, 67*), we found that most of the GFP-labeled S1/S2 axons projected to corresponding contralateral S1 and S1/S2 border regions in P14 mice, that expression of dnRab5b increased homotopic contralateral S1/S2 projections, and that a notable fraction of S1/S2 axons projected to the retrosplenial agranular (RSA) and retrosplenial granular (RSG) cortex, more medial regions to the contralateral S1/S2 cortex (Fig. 9, A to D, and Fig. S6B). Indeed, RSA/RSG regions are mainly innervated by axons from thalamus, subiculum, and postsubiculum, as well as contralateral RSA/RSG (*68, 69*). In contrast to the effect of dnRab5b, expression of wild-type Rab5b slightly decreased the contralateral RSA/RSG projections, without an apparent effect on the homotopic S1/S2 projections (Fig. 9, A to D). Thus, Rab5 plays an important role in proper targeting of callosal axons.

Next, we determined the role of NP1 in the contralateral projection of callosal axons. Embryos of *NP1*$^{f/f}$ mice were in utero–electroporated with plasmids expressing GFP, either alone or together with the Cre expression construct (ubiqutin-Cre-2A-GFP) into S1/S2 at E15.5, followed by examination at P14. We found that Cre-electroporated *NP1*$^{f/f}$ mice exhibited excessive contralateral axon projections, as reflected in increased contralateral projections to the homotopic S1/S2 regions as well as ectopic projections to the RSA/RSG regions (Fig. 10, A to D). This phenomenon phenocopied the effect caused by Rab5 inhibition. To further determine the relationship between NP1 and Rab5 in callosal axon projection, *NP1*$^{f/f}$ embryos were electroporated with vectors expressing Rab5b, together with Cre and GFP constructs. Notably, expression of Rab5b rescued the defects caused by *NP1* knockout (Fig. 10, A to D). These results are in line with the notion that Rab5 acts downstream of Sema3A signaling in refining callosal axon projections.

DISCUSSION

Sema3A induces growth cone collapse, repels growing axons, or inhibits axon development (*3, 10, 11, 14*). These activities are believed to confine axon projection pathways and drive axon trajectories to form fascicles (*7, 25*). However, the intracellular mechanism of Sema3A action remains unclear. Here, we show that Rab5, a member of the Rab family small

GTPases, which plays critical roles in endosome biogenesis and transportation (*29, 38, 70, 71*), acts downstream of Sema3A signaling in inducing growth cone collapse and sculpting axon projections.

In different cellular contexts, a number of molecules have been shown to be involved in Sema3A signaling, including kinases (*72–74*), Rho family of small G proteins (*22, 23, 75–77*), regulators for GTPases (*24, 78*), and actin or microtubule-associated proteins (*79–81*). Notably, Sema3A enhances endocytosis at sites of receptor–F-actin colocalization during growth cone collapse (*26*), and inhibition of clathrin-mediated endocytosis abolishes growth cone repulsion (*27*). It is unknown how Sema3A induces membrane endocytosis at axonal growth cones. By searching for proteins that interacted with Plexin-A1, the signal transduction subunit of the Sema3A holoreceptor, we identified Rabaptin-5, a direct effector of Rab5 that has been proposed to function as a molecular linker to coordinate endocytosis and recycling (*41, 49, 82, 83*). We found that Sema3A stimulation induced the recruitment of Rab5 to the Plexin-A1 complex and activated Rab5 in a Rabaptin-5–dependent manner in L2/3 neurons. Like other Rab proteins, Rab5 activity and localization should be regulated by various regulators, including GEFs, GAPs, or effectors (*28, 29*). As a Rab5 effector, Rabaptin-5 forms a complex with Rabex-5, which catalyzes nucleotide exchange on Rab5 (*41, 49, 82, 83*). Thus, we proposed a model that Rabaptin-5, through its interactions with Plexin-A1, Rab5, and regulatory molecules (such as Rabex-5), mediates the formation of a signaling complex. Upon Sema3A stimulation, Rab5 in membrane domains is activated, which triggers biogenesis of endosomes and membrane endocytosis. In line with this hypothesis, Rabex-5 was associated with Rabaptin-5, and Sema3A-mediated Rab5 activation in axonal growth cones requires Rabex-5.

To study the functional relevance of Sema3A-Rab5 signaling in axon patterning, we determined short-term and long-lasting effects of Rab5 or Rabaptin-5. In short-term assays, we found that Rab5 was essential for Sema3A-induced growth cone collapse, membrane endocytosis, and axon growth inhibition. As one of the best-studied repulsive factors, Sema3A is believed to define permissive pathways for axon trajectories by acting as a “stop” or “corridor” signal (*25*). However, the role of Sema3A signaling in axon bundling and projections of CNS remains elusive, although distribution of Sema3A and its receptors implicates this possibility (*21, 47, 48, 61*). In agreement with this possibility, we found that the Sema3A protein distribution was complementary to Smi312, which marked the callosal axon bundles. Through the analysis of mice with *NP1* knockout or expression of cytoPlexin-A1, which had been shown to be the dominant-negative construct for Sema3A signaling in growth cone collapse and membrane endocytosis, we found that loss of function of Sema3A signaling caused defasciculation and mistargeting of callosal axon trajectories. In line with the notion that Rab5 acts downstream of Sema3A signaling, inhibiting the function or decreasing the abundance of Rab5 phenocopied these axon bundling and targeting defects. Finally, the genetic relationship between Sema3A signaling and Rab5 activation was further consolidated by the findings that defasciculation of callosal axon bundles caused by cytoPlexin-A1 expression or *NP1* knockout, or ectopic targeting of contralateral axon trajectories in *NP1* knockout mice, was prevented by increased Rabaptin-5 or Rab5. These results indicate that Rab5 and Rabaptin-5 are in the downstream signaling of the NP1–

Plexin-A1 holoreceptor and are in line with the findings that Rab5 is essential for the role of Sema3A in triggering growth cone collapse and inhibiting cortical axon growth.

Semaphorin signaling often facilitates de-adhesion (*25*), and indeed, some cell adhesion molecules, such as L1 Ig superfamily adhesion molecule, are involved in semaphorin signaling and axon fasciculation (*54*, *84–86*). It would be interesting to establish the relationship between Rab5-mediated membrane endocytosis and surface distribution of adhesion molecules, and the subsequent growth cone dynamics. Several other guidance cues or morphogens, including Slit2, ephrins, Netrin1, or Wnt5a, have been shown to regulate callosal axon pathfinding (*87–92*). However, Slit2, EphrinA2, or Netrin1 did not regulate Rab5 activity. As a coordinator and timer of membrane endocytosis (*29*), Rab5 plays important roles in other neurological events, such as neocortical neuronal migration (*39*) and synaptic plasticity (*37*). The Sema3A regulation of Rab5 may also function in these processes. How Rab5 coordinates neuronal morphogenesis, positioning, and distribution of functional proteins is an important issue to be addressed.

MATERIALS AND METHODS

Reagents and antibodies

Recombinant human Sema3A was from R&D Systems. Alexa Fluor 555 dextran [10,000 molecular weight (MW)], Alexa Fluor 555 phalloidin, and FM4-64 were from Invitrogen. DAPI was from Beyotime. Glutathione Sepharose 4B was from GE Healthcare, Ni-NTA agarose was from Qiagen, and protein A– or protein G–agarose was from Roche. Lipofectamine 2000 transfection reagent was from Invitrogen. Antibodies were from Abcam (His, Ki67, NP1, Plexin-A1, Rab5, Satb2, Sema3A), Aves Labs (GFP, fluorescein-labeled goat anti-chicken IgY), BD Biosciences Pharmagen (Rab5, Rab8), Cell Signaling Technology (Rab7), Covance (Smi312), Invitrogen (GFP, Alexa Flour 488 goat anti-rabbit IgG, Alexa Flour 555 goat anti-mouse IgG), Millipore (actin, horseradish peroxidase–conjugated goat anti-rabbit or mouse IgG), ProteinTech Group (Rab5a, Rab5b, Rab5c, Rab10), Santa Cruz Biotechnology (Rabaptin-5, Rabex-5), and Sigma (HA).

Cell culture, transfection, and treatments

Upper-layer cortical tissues were dissociated from E17.5 SD rat brains. The dissociated cortical neurons were cultured on poly-D-lysine (PDL)–precoated glass coverslips or dishes in the plating medium composed of 80% Dulbecco's modified Eagle's medium (DMEM), 10% fetal bovine serum (FBS), and 10% F12. After 24 hours, the culture medium was changed into neuronal basal medium containing 2% B27 and 1% L-glutamine. Dissociated neurons were transfected by electroporation using Amaxa Nucleofector device before plating. HEK293 cells were transfected by Lipofectamine 2000 following the manufacturer's instructions. The morphology of axonal growth cones of $Satb2^+$ neurons was analyzed at 3 DIV. Sometimes, cultured neurons were treated with Sema3A (300 ng/ml).

Molecular biology and protein expression

Rat Rab5a, Rab5b, or Rab5c was amplified from rat complementary DNA (cDNA) using Pfu polymerase (Stratagene) and cloned into pKH3. Rab5b was also cloned into pCAGGS

vector (*93*). Rabaptin-5 was amplified from rat cDNA and cloned into pCS2+ or pET-32a vector. Cytoplasmic fragment of Plexin-A1 (1271 to 1894 amino acids) was amplified from the mouse Plexin-A1 cDNA (*20*) and subcloned into pKH3 or pGEX-2T vectors. The sequences for Rab5 siRNAs were as follows: 5′-GGAACGATACCACAGTTTA-3′ (siRab5b-503), 5′-GCGCATGGTGGAGTATGAA-3′ (siRab5b-686), 5′-GGCTCAGGCATATGCAGAT-3′ (siRab5b-707), 5′-GGCAAGCAAGTCCTAATAT-3′ (siRab5a#2), and 5′-TCATTGCACTAGCGGGTAA-3′ (siRab5c#2). The siRNA sequence targeting Rabaptin-5 was 5′-GCTTTAGGCTATAACTACA-3′ (*50*). The 19-mer oligonucleotides were annealed and cloned into pSUPER vector. As that shown previously (*51*), the siRNA oligos against Rabex-5 were synthesized by GenePharma, with the following sequence: 5′-GTTCAAGACATTGTTGAGA-3′. Rabaptin-5 and cytoplasmic fragment of Plexin-A1 (1271 to 1894 amino acids) were cloned into pET-32a and pGEX-2T, respectively, and expressed in *Escherichia coli* BL21 as His or GST fusion proteins, followed by affinity purification using Ni-NTA agarose (Qiagen) or Glutathione Sepharose 4B (GE Healthcare).

Immunoprecipitation and pull-down assay

HEK293 cells were cultured in DMEM containing 10% FBS and transfected with Lipofectamine 2000. Cell lysates were prepared in lysis buffer [25 mM tris-HCl (pH 7.5), 40 mM NaCl, 30 mM $MgCl_2$, 0.5% NP-40, 1 mM dithiothreitol (DTT), and cocktail protease inhibitors]. Immunoprecipitation was performed as described previously (*94*). GST-R5BD (*40*) or GST-cytoPlexin-A1 was expressed in *E. coli* strain BL21 and affinity-purified using Glutathione Sepharose 4B beads. Cultured cortical neurons, HEK293 cells, or rat brain homogenates were lysed in the lysis buffer containing 25 mM Hepes (pH 7.4), 100 mM NaCl, 5 mM $MgCl_2$, 0.1% NP-40, 10% glycerol, protease inhibitor cocktail, and 1 mM DTT. Lysates were clarified by centrifugation at 12,000 rpm for 15 min at 4°C. The supernatants were collected and incubated with beads coupled with GST-R5BD fusion proteins or GST–cytoPlexin-A1 proteins at 4°C overnight in the buffer containing 25 mM tris-HCl (pH 7.5), 40 mM NaCl, 30 mM $MgCl_2$, 0.5% NP-40, 20 nM GTPγS, 1 mM DTT, and cocktail protease inhibitors. The beads were then washed with the lysis buffer and subjected to SDS– polyacrylamide gel electrophoresis (SDS-PAGE) and immunoblotting. Band intensity was measured using National Institutes of Health ImageJ 1.47a software.

Endocytosis assay

For dextran endocytosis assay, cultured neurons at 3 DIV were incubated for 15 min at 37°C in the medium containing Alexa Fluor 555 dextran (10,000 MW, 2 mg/ml) or FM4-64 (5 μg/ml), without or with Sema3A, and then washed with phosphate-buffered saline (PBS) and fixed with 4% paraformaldehyde (PFA) for 20 min at room temperature in darkness for microscopic analysis.

Stripe coating and microfluidic culture system

PDMS (polydimethylsiloxane) molds, which contained a series of 60-μm-width parallel microgrooves separated by 100-μm gaps, were fabricated as described previously (*62*) and pressed onto PDL-coated coverslips; thus, the microchannels formed between the PDMS

molds and the coverslips. Then, Sema3A (600 ng/ml), mixed with Alexa 555–conjugated bovine serum albumin (1:1000), was added to microchannels and incubated at 4°C overnight. The adsorbed protein stripes were formed when PDMS molds were removed, and were ready for cell plating.

The two-compartment microfluidic culture devices were prepared using soft lithography as reported previously (*63*). PDMS microfluidic chips were fabricated by replica-molding-curing a liquid mixture of degassed silicone elastomer and curing agent (weight ratio 10:1) on the master silicon wafer, and then peeled off and cut into square chips with microgrooves (3 μm high, 10 μm wide, and 100 μm long) between two compartments (100 μm high, 1500 μm wide, and 8 μm long), and, after sterilization, were pressed onto PDL-coated coverslips. Cells were seeded into the chamber linking the somatodendritic compartment. To create repulsive environment, Sema3A (300 ng/ml) was added to the chamber linking the axonal compartment.

Immunostaining

Cultured neurons were washed with PBS, then fixed with 4% PFA for 20 min, and penetrated by treatment with 0.1% Triton X-100 for 15 min. Cells were incubated in primary antibodies at 4°C overnight, and subsequently fluorescence-labeled secondary antibodies. Working solution of DAPI or phalloidin was applied directly to the samples for 20 to 30 min at room temperature. For the staining with GST-R5BD, fixed neurons were incubated with purified GST-R5BD protein (0.5 μg/ml) at 4°C overnight, then washed with PBS, and incubated with primary antibody recognizing GST. Cryostat sections of brain slices were incubated in 0.3% Triton X-100 for 30 min and 10% goat serum in PBS for 1 hour at room temperature, followed by staining with primary antibodies at 4°C overnight and subsequent secondary antibodies for 2 hours at room temperature.

In utero electroporation

In utero electroporation was performed as described previously (*93*). Briefly, interested plasmids (5 μg for rats and 3 μg for mice) mixed with Fast Green were injected into the lateral ventricle of the embryonic brains, which were then subjected to electroporation consisting of five square wave pulses with fixed amplitude (60 V for rats, 36 V for mice), a duration of 50 ms, and an interval of 1 s (ECM 830; BTX). Brains of postnatal pups at indicated times were sectioned, stained, and observed under fluorescent microscope. All animal usage followed guidelines by the Institutional Animal Care and Use Committee of Institute of Neuroscience, Chinese Academy of Sciences.

Confocal imaging and data analysis

Images of axonal growth cones were imaged by Nikon A1R laser scanning confocal microscopy with a Plan Apo VC 60× oil objective with numerical aperture 1.4. Brain slices were imaged by Neurolucida with Plan Apo 10× objective or Nikon A1R with a Plan Apo 10× objective. For colocalization analysis, the Pearson's correlation coefficient and % voxels of colocalization were obtained from both channels with ImageJ plugin "Colocalization analysis—colocalization threshold." Data analysis was performed with ANOVA with post hoc or Student's *t* test. Errors bars in graphs represent SEM.

Supplementary Material

Refer to Web version on PubMed Central for supplementary material.

Acknowledgments

We are grateful to S. M. Strittmatter for the Plexin-A1 construct, and A. L. Kolodkin and X. B. Yuan for the *NP1 floxed* mice. We thank Q. Hu of ION Imaging Facility for the microscope analysis and J. Zhou for sharing the ubiqutin-Cre-2A-GFP plasmid. **Funding:** This work was partially supported by the Key State Research Program (2014CB910203 to Z.-G.L.), the National Natural Science Foundation of China (31371063 to K.-Y.W.; 31330032, 31321091, and 61327902 to Z.-G.L.; and 21025520 to X.-Y.J.), the Knowledge Innovation Program of Shanghai Institutes for Biological Sciences, the Chinese Academy of Sciences (2013KIP206 to K.-Y.W.), and NIH (R01GM074692 to G.L.).

REFERENCES

1. Kolodkin AL, Tessier-Lavigne M. Mechanisms and molecules of neuronal wiring: A primer. Cold Spring Harb. Perspect. Biol. 2011; 3:a001727. [PubMed: 21123392]
2. Raper J, Mason C. Cellular strategies of axonal pathfinding. Cold Spring Harb. Perspect. Biol. 2010; 2:a001933. [PubMed: 20591992]
3. Luo Y, Raible D, Raper JA. Collapsin: A protein in brain that induces the collapse and paralysis of neuronal growth cones. Cell. 1993; 75:217–227. [PubMed: 8402908]
4. Polleux F, Giger RJ, Ginty DD, Kolodkin AL, Ghosh A. Patterning of cortical efferent projections by semaphorin-neuropilin interactions. Science. 1998; 282:1904–1906. [PubMed: 9836643]
5. Bagnard D, Lohrum M, Uziel D, Püschel AW, Bolz J. Semaphorins act as attractive and repulsive guidance signals during the development of cortical projections. Development. 1998; 125:5043–5053. [PubMed: 9811588]
6. Fan J, Raper JA. Localized collapsing cues can steer growth cones without inducing their full collapse. Neuron. 1995; 14:263–274. [PubMed: 7857638]
7. Raper JA. Semaphorins and their receptors in vertebrates and invertebrates. Curr. Opin. Neurobiol. 2000; 10:88–94. [PubMed: 10679438]
8. Chen G, Sima J, Jin M, Wang KY, Xue XJ, Zheng W, Ding YQ, Yuan XB. Semaphorin-3A guides radial migration of cortical neurons during development. Nat. Neurosci. 2008; 11:36–44. [PubMed: 18059265]
9. Polleux F, Morrow T, Ghosh A. Semaphorin 3A is a chemoattractant for cortical apical dendrites. Nature. 2000; 404:567–573. [PubMed: 10766232]
10. Nishiyama M, Togashi K, von Schimmelmann MJ, Lim CS, Maeda S, Yamashita N, Goshima Y, Ishii S, Hong K. Semaphorin 3A induces $Ca_V2.3$ channel-dependent conversion of axons to dendrites. Nat. Cell Biol. 2011; 13:676–685. [PubMed: 21602796]
11. Shelly M, Cancedda L, Lim BK, Popescu AT, Cheng PL, Gao H, Poo MM. Semaphorin3A regulates neuronal polarization by suppressing axon formation and promoting dendrite growth. Neuron. 2011; 71:433–446. [PubMed: 21835341]
12. Morita A, Yamashita N, Sasaki Y, Uchida Y, Nakajima O, Nakamura F, Yagi T, Taniguchi M, Usui H, Katoh-Semba R, Takei K, Goshima Y. Regulation of dendritic branching and spine maturation by semaphorin3A-Fyn signaling. J. Neurosci. 2006; 26:2971–2980. [PubMed: 16540575]
13. Yamashita N, Morita A, Uchida Y, Nakamura F, Usui H, Ohshima T, Taniguchi M, Honnorat J, Thomasset N, Takei K, Takahashi T, Kolattukudy P, Goshima Y. Regulation of spine development by semaphorin3A through cyclin-dependent kinase 5 phosphorylation of collapsin response mediator protein 1. J. Neurosci. 2007; 27:12546–12554. [PubMed: 18003833]
14. Behar O, Golden JA, Mashimo H, Schoen FJ, Fishman MC. Semaphorin III is needed for normal patterning and growth of nerves, bones and heart. Nature. 1996; 383:525–528. [PubMed: 8849723]
15. Kitsukawa T, Shimizu M, Sanbo M, Hirata T, Taniguchi M, Bekku Y, Yagi T, Fujisawa H. Neuropilin–semaphorin III/D-mediated chemorepulsive signals play a crucial role in peripheral nerve projection in mice. Neuron. 1997; 19:995–1005. [PubMed: 9390514]

16. Taniguchi M, Yuasa S, Fujisawa H, Naruse I, Saga S, Mishina M, Yagi T. Disruption of semaphorin III/D gene causes severe abnormality in peripheral nerve projection. Neuron. 1997; 19:519–530. [PubMed: 9331345]
17. Feiner L, Koppel AM, Kobayashi H, Raper JA. Secreted chick semaphorins bind recombinant neuropilin with similar affinities but bind different subsets of neurons in situ. Neuron. 1997; 19:539–545. [PubMed: 9331347]
18. He Z, Tessier-Lavigne M. Neuropilin is a receptor for the axonal chemorepellent Semaphorin III. Cell. 1997; 90:739–751. [PubMed: 9288753]
19. Kolodkin AL, Levengood DV, Rowe EG, Tai YT, Giger RJ, Ginty DD. Neuropilin is a semaphorin III receptor. Cell. 1997; 90:753–762. [PubMed: 9288754]
20. Takahashi T, Fournier A, Nakamura F, Wang LH, Murakami Y, Kalb RG, Fujisawa H, Strittmatter SM. Plexin-neuropilin-1 complexes form functional semaphorin-3A receptors. Cell. 1999; 99:59–69. [PubMed: 10520994]
21. Gu C, Rodriguez ER, Reimert DV, Shu T, Fritzsch B, Richards LJ, Kolodkin AL, Ginty DD. Neuropilin-1 conveys semaphorin and VEGF signaling during neural and cardiovascular development. Dev. Cell. 2003; 5:45–57. [PubMed: 12852851]
22. Jin Z, Strittmatter SM. Rac1 mediates collapsin-1-induced growth cone collapse. J. Neurosci. 1997; 17:6256–6263. [PubMed: 9236236]
23. Jurney WM, Gallo G, Letourneau PC, McLoon SC. Rac1-mediated endocytosis during ephrin-A2- and semaphorin 3A-induced growth cone collapse. J. Neurosci. 2002; 22:6019–6028. [PubMed: 12122063]
24. Toyofuku T, Yoshida J, Sugimoto T, Zhang H, Kumanogoh A, Hori M, Kikutani H. FARP2 triggers signals for Sema3A-mediated axonal repulsion. Nat. Neurosci. 2005; 8:1712–1719. [PubMed: 16286926]
25. Tran TS, Kolodkin AL, Bharadwaj R. Semaphorin regulation of cellular morphology. Annu. Rev. Cell Dev. Biol. 2007; 23:263–292. [PubMed: 17539753]
26. Fournier AE, Nakamura F, Kawamoto S, Goshima Y, Kalb RG, Strittmatter SM. Semaphorin3A enhances endocytosis at sites of receptor–F-actin colocalization during growth cone collapse. J. Cell Biol. 2000; 149:411–422. [PubMed: 10769032]
27. Tojima T, Itofusa R, Kamiguchi H. Asymmetric clathrin-mediated endocytosis drives repulsive growth cone guidance. Neuron. 2010; 66:370–377. [PubMed: 20471350]
28. Stenmark H. Rab GTPases as coordinators of vesicle traffic. Nat. Rev. Mol. Cell Biol. 2009; 10:513–525. [PubMed: 19603039]
29. Zerial M, McBride H. Rab proteins as membrane organizers. Nat. Rev. Mol. Cell Biol. 2001; 2:107–117. [PubMed: 11252952]
30. Chavrier P, Parton RG, Hauri HP, Simons K, Zerial M. Localization of low molecular weight GTP binding proteins to exocytic and endocytic compartments. Cell. 1990; 62:317–329. [PubMed: 2115402]
31. Gorvel JP, Chavrier P, Zerial M, Gruenberg J. rab5 controls early endosome fusion in vitro. Cell. 1991; 64:915–925. [PubMed: 1900457]
32. Rybin V, Ullrich O, Rubino M, Alexandrov K, Simon I, Seabra MC, Goody R, Zerial M. GTPase activity of Rab5 acts as a timer for endocytic membrane fusion. Nature. 1996; 383:266–269. [PubMed: 8805704]
33. Nielsen E, Severin F, Backer JM, Hyman AA, Zerial M. Rab5 regulates motility of early endosomes on microtubules. Nat. Cell Biol. 1999; 1:376–382. [PubMed: 10559966]
34. Bucci C, Parton RG, Mather IH, Stunnenberg H, Simons K, Hoflack B, Zerial M. The small GTPase rab5 functions as a regulatory factor in the early endocytic pathway. Cell. 1992; 70:715–728. [PubMed: 1516130]
35. Pfeffer SR. Rab GTPases: Specifying and deciphering organelle identity and function. Trends Cell Biol. 2001; 11:487–491. [PubMed: 11719054]
36. de Hoop MJ, Huber LA, Stenmark H, Williamson E, Zerial M, Parton RG, Dotti CG. The involvement of the small GTP-binding protein Rab5a in neuronal endocytosis. Neuron. 1994; 13:11–22. [PubMed: 8043272]

37. Brown TC, Tran IC, Backos DS, Esteban JA. NMDA receptor-dependent activation of the small GTPase Rab5 drives the removal of synaptic AMPA receptors during hippocampal LTD. Neuron. 2005; 45:81–94. [PubMed: 15629704]

38. Deinhardt K, Salinas S, Verastegui C, Watson R, Worth D, Hanrahan S, Bucci C, Schiavo G. Rab5 and Rab7 control endocytic sorting along the axonal retrograde transport pathway. Neuron. 2006; 52:293–305. [PubMed: 17046692]

39. Kawauchi T, Sekine K, Shikanai M, Chihama K, Tomita K, Kubo K, Nakajima K, Nabeshima Y, Hoshino M. Rab GTPases-dependent endocytic pathways regulate neuronal migration and maturation through N-cadherin trafficking. Neuron. 2010; 67:588–602. [PubMed: 20797536]

40. Liu J, Lamb D, Chou MM, Liu YJ, Li G. Nerve growth factor-mediated neurite outgrowth via regulation of Rab5. Mol. Biol. Cell. 2007; 18:1375–1384.

41. Stenmark H, Vitale G, Ullrich O, Zerial M. Rabaptin-5 is a direct effector of the small GTPase Rab5 in endocytic membrane fusion. Cell. 1995; 83:423–432. [PubMed: 8521472]

42. Mitchell BD, Macklis JD. Large-scale maintenance of dual projections by callosal and frontal cortical projection neurons in adult mice. J. Comp. Neurol. 2005; 482:17–32. [PubMed: 15612019]

43. Fame RM, MacDonald JL, Macklis JD. Development, specification, and diversity of callosal projection neurons. Trends Neurosci. 2011; 34:41–50. [PubMed: 21129791]

44. Yang T, Terman JR. 14-3-3e couples protein kinase A to Semaphorin signaling and silences plexin RasGAP-mediated axonal repulsion. Neuron. 2012; 74:108–121. [PubMed: 22500634]

45. Alcamo EA, Chirivella L, Dautzenberg M, Dobreva G, Fariñas I, Grosschedl R, McConnell SK. Satb2 regulates callosal projection neuron identity in the developing cerebral cortex. Neuron. 2008; 57:364–377. [PubMed: 18255030]

46. Britanova O, de Juan Romero C, Cheung A, Kwan KY, Schwark M, Gyorgy A, Vogel T, Akopov S, Mitkovski M, Agoston D, Sestan N, Molnár Z, Tarabykin V. Satb2 is a postmitotic determinant for upper-layer neuron specification in the neocortex. Neuron. 2008; 57:378–392. [PubMed: 18255031]

47. Piper M, Plachez C, Zalucki O, Fothergill T, Goudreau G, Erzurumlu R, Gu C, Richards LJ. Neuropilin 1-Sema signaling regulates crossing of cingulate pioneering axons during development of the corpus callosum. Cereb. Cortex. 2009; 19(Suppl. 1):i11–i21. [PubMed: 19357391]

48. Zhou J, Wen Y, She L, Sui YN, Liu L, Richards LJ, Poo MM. Axon position within the corpus callosum determines contralateral cortical projection. Proc. Natl. Acad. Sci. U.S.A. 2013; 110:E2714–E2723. [PubMed: 23812756]

49. Vitale G, Rybin V, Christoforidis S, Thornqvist P, McCaffrey M, Stenmark H, Zerial M. Distinct Rab-binding domains mediate the interaction of Rabaptin-5 with GTP-bound rab4 and rab5. EMBO J. 1998; 17:1941–1951. [PubMed: 9524117]

50. Rios EJ, Piliponsky AM, Ra C, Kalesnikoff J, Galli SJ. Rabaptin-5 regulates receptor expression and functional activation in mast cells. Blood. 2008; 112:4148–4157. [PubMed: 18698003]

51. Mori Y, Matsui T, Fukuda M. Rabex-5 protein regulates dendritic localization of small GTPase Rab17 and neurite morphogenesis in hippocampal neurons. J. Biol. Chem. 2013; 288:9835–9847. [PubMed: 23430262]

52. Tamagnone L, Artigiani S, Chen H, He Z, Ming GI, Song H, Chedotal A, Winberg ML, Goodman CS, Poo M, Tessier-Lavigne M, Comoglio PM. Plexins are a large family of receptors for transmembrane, secreted, and GPI-anchored semaphorins in vertebrates. Cell. 1999; 99:71–80. [PubMed: 10520995]

53. Gorski JA, Talley T, Qiu M, Puelles L, Rubenstein JL, Jones KR. Cortical excitatory neurons and glia, but not GABAergic neurons, are produced in the Emx1-expressing lineage. J. Neurosci. 2002; 22:6309–6314. [PubMed: 12151506]

54. Bechara A, Nawabi H, Moret F, Yaron A, Weaver E, Bozon M, Abouzid K, Guan JL, Tessier-Lavigne M, Lemmon V, Castellani V. FAK–MAPK-dependent adhesion disassembly downstream of L1 contributes to semaphorin3A-induced collapse. EMBO J. 2008; 27:1549–1562. [PubMed: 18464795]

55. Pozas E, Pascual M, Nguyen Ba-Charvet KT, Guijarro P, Sotelo C, Chédotal A, Del Río JA, Soriano E. Age-dependent effects of secreted Semaphorins 3A, 3F, and 3E on developing

hippocampal axons: In vitro effects and phenotype of Semaphorin 3A (−/−) mice. Mol. Cell. Neurosci. 2001; 18:26–43. [PubMed: 11461151]

56. Qin Q, Liao G, Baudry M, Bi X. Role of calpain-mediated p53 truncation in semaphorin 3A-induced axonal growth regulation. Proc. Natl. Acad. Sci. U.S.A. 2010; 107:13883–13887.
57. Kabayama H, Takeuchi M, Taniguchi M, Tokushige N, Kozaki S, Mizutani A, Nakamura T, Mikoshiba K. Syntaxin 1B suppresses macropinocytosis and semaphorin 3A-induced growth cone collapse. J. Neurosci. 2011; 31:7357–7364. [PubMed: 21593320]
58. Mikule K, Gatlin JC, de la Houssaye BA, Pfenninger KH. Growth cone collapse induced by semaphorin 3A requires 12/15-lipoxygenase. J. Neurosci. 2002; 22:4932–4941. [PubMed: 12077190]
59. Vida TA, Emr SD. A new vital stain for visualizing vacuolar membrane dynamics and endocytosis in yeast. J. Cell Biol. 1995; 128:779–792. [PubMed: 7533169]
60. Lindwall C, Fothergill T, Richards LJ. Commissure formation in the mammalian. forebrain. Curr. Opin. Neurobiol. 2007; 17:3–14. [PubMed: 17275286]
61. Piper M, Moldrich RX, Lindwall C, Little E, Barry G, Mason S, Sunn N, Kurniawan ND, Gronostajski RM, Richards LJ. Multiple non-cell-autonomous defects underlie neocortical callosal dysgenesis in Nfib-deficient mice. Neural Dev. 2009; 4:43. [PubMed: 19961580]
62. Walter J, Kern-Veits B, Huf J, Stolze B, Bonhoeffer F. Recognition of position-specific properties of tectal cell membranes by retinal axons in vitro. Development. 1987; 101:685–696. [PubMed: 3503693]
63. Taylor AM, Blurton-Jones M, Rhee SW, Cribbs DH, Cotman CW, Jeon NL. A microfluidic culture platform for CNS axonal injury, regeneration and transport. Nat. Methods. 2005; 2:599–605. [PubMed: 16094385]
64. Erskine L, Reijntjes S, Pratt T, Denti L, Schwarz Q, Vieira JM, Alakakone B, Shewan D, Ruhrberg C. VEGF signaling through neuropilin 1 guides commissural axon crossing at the optic chiasm. Neuron. 2011; 70:951–965. [PubMed: 21658587]
65. Ulupinar E, Datwani A, Behar O, Fujisawa H, Erzurumlu R. Role of semaphorin III in the developing rodent trigeminal system. Mol. Cell. Neurosci. 1999; 13:281–292. [PubMed: 10328887]
66. Molyneaux BJ, Arlotta P, Menezes JR, Macklis JD. Neuronal subtype specification in the cerebral cortex. Nat. Rev. Neurosci. 2007; 8:427–437. [PubMed: 17514196]
67. Wise SP, Jones EG. The organization and postnatal development of the commissural projection of the rat somatic sensory cortex. J. Comp. Neurol. 1976; 168:313–343. [PubMed: 950383]
68. Vann SD, Aggleton JP, Maguire EA. What does the retrosplenial cortex do? Nat. Rev. Neurosci. 2009; 10:792–802. [PubMed: 19812579]
69. Van Groen T, Wyss JM. Connections of the retrosplenial granular b cortex in the rat. J. Comp. Neurol. 2003; 463:249–263. [PubMed: 12820159]
70. Rink J, Ghigo E, Kalaidzidis Y, Zerial M. Rab conversion as a mechanism of progression from early to late endosomes. Cell. 2005; 122:735–749. [PubMed: 16143105]
71. Sönnichsen B, De Renzis S, Nielsen E, Rietdorf J, Zerial M. Distinct membrane domains on endosomes in the recycling pathway visualized by multicolor imaging of Rab4, Rab5, and Rab11. J. Cell Biol. 2000; 149:901–914. [PubMed: 10811830]
72. Aizawa H, Wakatsuki S, Ishii A, Moriyama K, Sasaki Y, Ohashi K, Sekine-Aizawa Y, Sehara-Fujisawa A, Mizuno K, Goshima Y, Yahara I. Phosphorylation of cofilin by LIM-kinase is necessary for semaphorin 3A-induced growth cone collapse. Nat. Neurosci. 2001; 4:367–373. [PubMed: 11276226]
73. Eickholt BJ, Walsh FS, Doherty P. An inactive pool of GSK-3 at the leading edge of growth cones is implicated in Semaphorin 3A signaling. J. Cell Biol. 2002; 157:211–217. [PubMed: 11956225]
74. Sasaki Y, Cheng C, Uchida Y, Nakajima O, Ohshima T, Yagi T, Taniguchi M, Nakayama T, Kishida R, Kudo Y, Ohno S, Nakamura F, Goshima Y. Fyn and Cdk5 mediate semaphorin-3A signaling, which is involved in regulation of dendrite orientation in cerebral cortex. Neuron. 2002; 35:907–920. [PubMed: 12372285]
75. Turner LJ, Nicholls S, Hall A. The activity of the Plexin-A1 receptor is regulated by Rac. J. Biol. Chem. 2004; 279:33199–33205. [PubMed: 15187088]

76. Wu KY, Hengst U, Cox LJ, Macosko EZ, Jeromin A, Urquhart ER, Jaffrey SR. Local translation of RhoA regulates growth cone collapse. Nature. 2005; 436:1020–1024. [PubMed: 16107849]
77. Zanata SM, Hovatta I, Rohm B, P schel AW. Antagonistic effects of Rnd1 and RhoD GTPases regulate receptor activity in Semaphorin 3A-induced cytoskeletal collapse. J. Neurosci. 2002; 22:471–477. [PubMed: 11784792]
78. Togashi H, Schmidt EF, Strittmatter SM. RanBPM contributes to Semaphorin3A signaling through Plexin-A receptors. J. Neurosci. 2006; 26:4961–4969. [PubMed: 16672672]
79. Deo RC, Schmidt EF, Elhabazi A, Togashi H, Burley SK, Strittmatter SM. Structural bases for CRMP function in plexin-dependent semaphorin3A signaling. EMBO J. 2004; 23:9–22. [PubMed: 14685275]
80. Gallo G. RhoA-kinase coordinates F-actin organization and myosin II activity during semaphorin-3A-induced axon retraction. J. Cell Sci. 2006; 119:3413–3423. [PubMed: 16899819]
81. Goshima Y, Nakamura F, Strittmatter P, Strittmatter SM. Collapsin-induced growth cone collapse mediated by an intracellular protein related to UNC-33. Nature. 1995; 376:509–514. [PubMed: 7637782]
82. Lippé R, Miaczynska M, Rybin V, Runge A, Zerial M. Functional synergy between Rab5 effector Rabaptin-5 and exchange factor Rabex-5 when physically associated in a complex. Mol. Biol. Cell. 2001; 12:2219–2228. [PubMed: 11452015]
83. Zhu G, Zhai P, Liu J, Terzyan S, Li G, Zhang XC. Structural basis of Rab5-Rabaptin5 interaction in endocytosis. Nat. Struct. Mol. Biol. 2004; 11:975–983. [PubMed: 15378032]
84. Demyanenko GP, Tsai AY, Maness PF. Abnormalities in neuronal process extension, hippocampal development, and the ventricular system of L1 knockout mice. J. Neurosci. 1999; 19:4907–4920. [PubMed: 10366625]
85. Castellani V, De Angelis E, Kenwrick S, Rougon G. Cis and trans interactions of L1 with neuropilin-1 control axonal responses to semaphorin 3A. EMBO J. 2002; 21:6348–6357. [PubMed: 12456642]
86. Wiencken-Barger AE, Mavity-Hudson J, Bartsch U, Schachner M, Casagrande VA. The role of L1 in axon pathfinding and fasciculation. Cereb. Cortex. 2004; 14:121–131. [PubMed: 14704209]
87. Shu T, Sundaresan V, McCarthy MM, Richards LJ. Slit2 guides both precrossing and postcrossing callosal axons at the midline in vivo. J. Neurosci. 2003; 23:8176–8184. [PubMed: 12954881]
88. Mendes SW, Henkemeyer M, Liebl DJ. Multiple Eph receptors and B-class ephrins regulate midline crossing of corpus callosum fibers in the developing mouse forebrain. J. Neurosci. 2006; 26:882–892. [PubMed: 16421308]
89. Keeble TR, Halford MM, Seaman C, Kee N, Macheda M, Anderson RB, Stacker SA, Cooper HM. The Wnt receptor Ryk is required for Wnt5a-mediated axon guidance on the contralateral side of the corpus callosum. J. Neurosci. 2006; 26:5840–5848. [PubMed: 16723543]
90. Li L, Hutchins BI, Kalil K. Wnt5a induces simultaneous cortical axon outgrowth and repulsive axon guidance through distinct signaling mechanisms. J. Neurosci. 2009; 29:5873–5883. [PubMed: 19420254]
91. Fazeli A, Dickinson SL, Hermiston ML, Tighe RV, Steen RG, Small CG, Stoeckli ET, Keino-Masu K, Masu M, Rayburn H, Simons J, Bronson RT, Gordon JI, Tessier-Lavigne M, Weinberg RA. Phenotype of mice lacking functional Deleted in colorectal cancer (Dcc) gene. Nature. 1997; 386:796–804. [PubMed: 9126737]
92. Serafini T, Colamarino SA, Leonardo ED, Wang H, Beddington R, Skarnes WC, Tessier-Lavigne M. Netrin-1 is required for commissural axon guidance in the developing vertebrate nervous system. Cell. 1996; 87:1001–1014. [PubMed: 8978605]
93. Saito T, Nakatsuji N. Efficient gene transfer into the embryonic mouse brain using in vivo electroporation. Dev. Biol. 2001; 240:237–246. [PubMed: 11784059]
94. Wang T, Liu Y, Xu XH, Deng CY, Wu KY, Zhu J, Fu XQ, He M, Luo ZG. Lg| 1 activation of Rab 10 promotes axonal membrane trafficking underlying neuronal polarization. Dev. Cell. 2011; 21:431–444. [PubMed: 21856246]

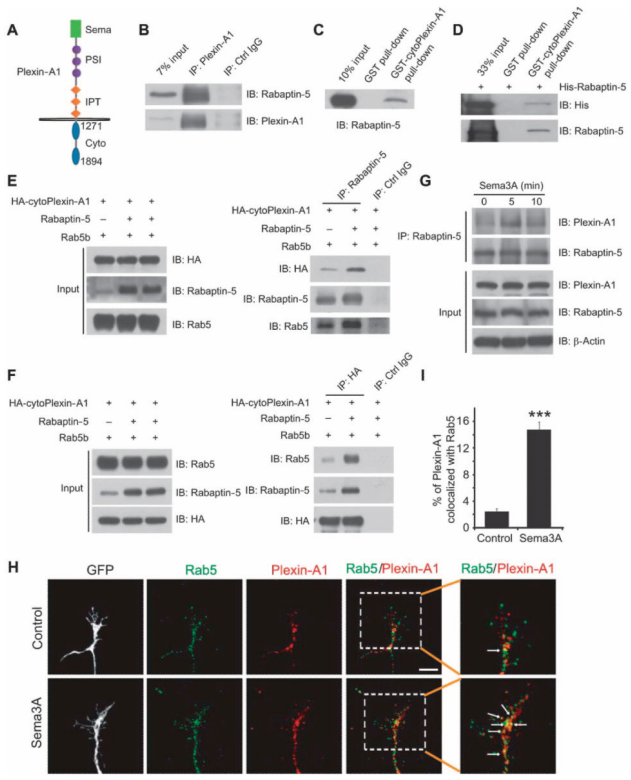

Fig. 1. Rabaptin-5 interacts with Plexin-A1

(**A**) Schematic illustration of mouse Plexin-A1 protein consisting of Sema, PSI (plexin-semaphorin-integrin), and IPT [immunoglobulin (Ig)–like, plexins, transcription factor] extracellular domains, and the transmembrane and intracellular domains. (**B**) Immunoblots for coimmunoprecipitation of Rabaptin-5 with Plexin-A1 in homogenate of postnatal day 5 (P5) rat upper cortical layers. Blots are representatives of three experiments. Ctrl, control. (**C**) Pull-down of Rabaptin-5 expressed in HEK293 cells by GST–cytoPlexin-A1 or GST beads. Blot is representative of three experiments. (**D**) Pull-down of purified His-tagged Rabaptin-5 by GST–cytoPlexin-A1 or GST beads. Blots are representatives of five experiments. (**E** and **F**) Immunoblots for cytoPlexin-A1 (by the HA tag), Rabaptin-5, and Rab5b before (Input) and after immunoprecipitation for Rabaptin-5 (E) or HA (F) in the lysates from HEK293 cells. Blots are representatives of five experiments. (**G**) Immunoblots for Rabaptin-5 and Plexin-A1 after immunoprecipitation for Rabaptin-5 in cultured cortical neurons treated with Sema3A (300 ng/ml) for indicated times. Blots are representatives of three experiments. (**H** and **I**) Immunostaining analysis for colocalization between endogenous Rab5 and Plexin-A1 in cultured L2/3 cortical neurons transfected with GFP, without or with treatment with Sema3A (300 ng/ml, 5 min). Data are means ± SEM from three experiments (29 neurons for control and 34 neurons for Sema3A). ***$P < 0.001$, Student's *t* test. Scale bar, 5 μm.

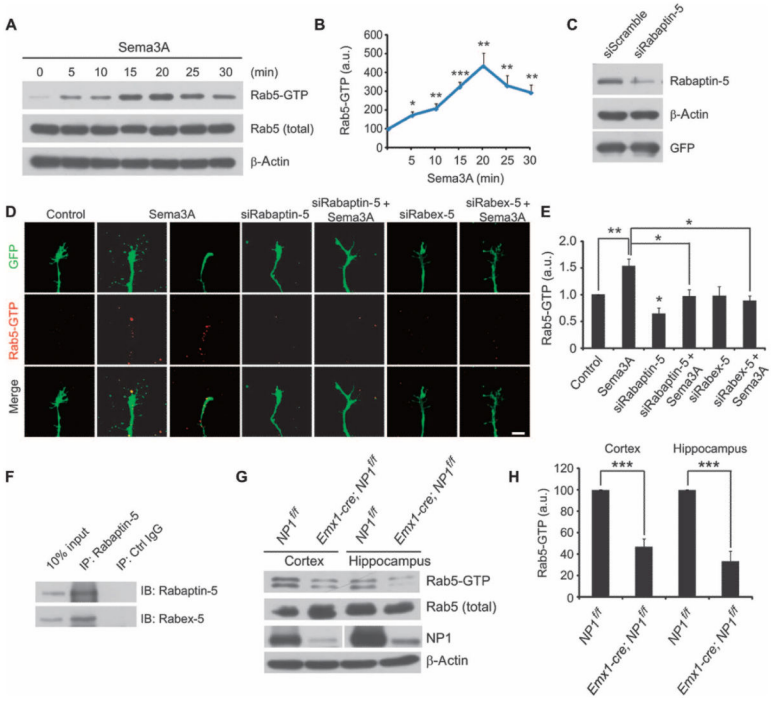

Fig. 2. Sema3A signaling activates Rab5

(**A** and **B**) Abundance of Rab5-GTP determined by pull-down using GST-R5BD in 3 DIV (days in vitro) L2/3 neurons treated with Sema3A (300 ng/ml) for the indicated time. Data are means ± SEM for the ratio of Rab5-GTP and total Rab5 from three experiments, normalized to control. **P* < 0.05, ***P* < 0.01, ****P* < 0.001, one-way ANOVA (analysis of variance) with Tukey HSD (honestly significant difference) post hoc test. a.u., arbitrary units. (**C**) Immunoblots for the efficiency of siRabaptin-5 in cultured cortical neurons with endogenous b-actin and vehicle-encoded GFP as loading controls. (**D** and **E**) Rab5-GTP marked by GST-R5BD in axonal growth cones of $Satb2^{+}$ L2/3 neurons transfected with scrambled (control) or indicated siRNAs, treated with vehicle or Sema3A (300 ng/ml, 15 min). Vector-encoded GFP was used to mark growth cone morphology and volume. Data are means ± SEM from at least 23 neurons from three experiments. **P* < 0.05, ***P* < 0.01, two-way ANOVA with post hoc comparisons using the Bonferroni correction. Scale bar, 10 μm. (**F**) Immunoblots for Rabaptin-5 and Rabex-5 after immunoprecipitation for Rabaptin-5 from homogenates of P5 rat upper-layer cortex. Blots are representatives of five experiments. (**G** and **H**) Immunoblots for the abundance of Rab5-GTP in the cortex or hippocampus from P30 mice with indicated genotypes. Data are means ± SEM of three experiments. ****P* < 0.001, one-way ANOVA with Tukey HSD post hoc test.

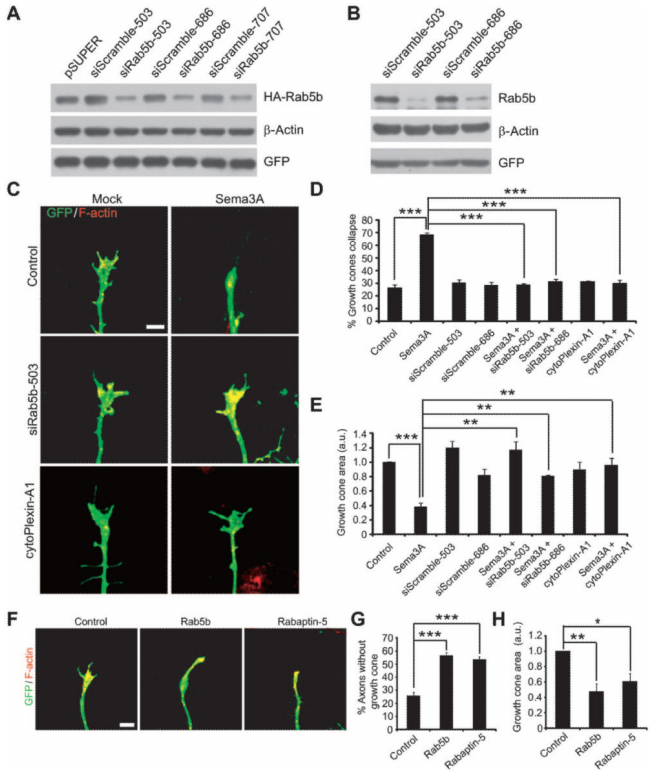

Fig. 3. Role of Rab5b in growth cone dynamics

(**A** and **B**) Immunoblots for the efficiencies of indicated siRNAs on the abundance of ectopic HA-Rab5b in the lysates of HEK293 cells (A) or endogenous Rab5b in cultured cortical neurons (B), with vectors encoding corresponding scrambled sequences as controls. Blots are representatives of three experiments. (**C** to **E**) Analysis for axonal growth cones of Satb2$^+$ L2/3 neurons transfected with indicated vectors treated with or without Sema3A (300 ng/ml, 15 min). F-actin was marked by Alexa Fluor 555 phalloidin (C). Data are means ± SEM for the percentage of collapsed growth cones (D) or normalized growth cone area (E) from three experiments. ***P* < 0.01, ****P* < 0.001, two-way ANOVA with Bonferroni correction post hoc test. Scale bar, 10 μm. (**F** to **H**) Analysis for axonal growth cones of Satb2$^+$ L2/3 neurons transfected with indicated constructs. Data are means ± SEM for the percentage of axons without apparent growth cones (G) or normalized growth cone area (H) from three experiments. **P* < 0.05, ***P* < 0.01, ****P* < 0.001, one-way ANOVA with Tukey HSD post hoc test. Scale bar, 10 μm.

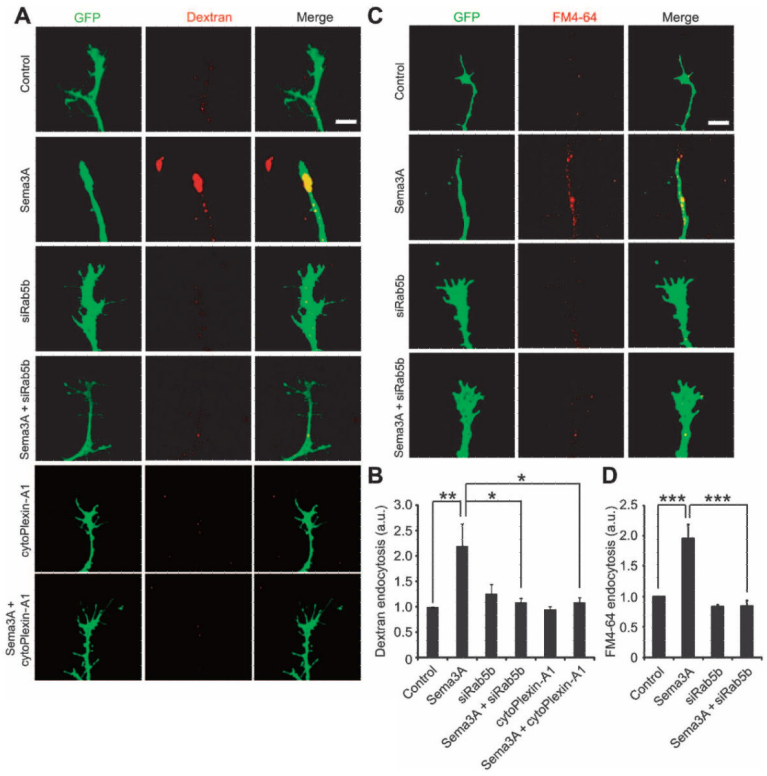

Fig. 4. Silencing of Rab5 impedes Sema3A-induced membrane endocytosis

(**A** and **C**) Cultured L2/3 neurons transfected with indicated plasmids were incubated with Alexa-labeled dextran (A) or FM4-64 (C), in the presence or absence of Sema3A for 15 min. Vehicle plasmids (A) or pSUPER encoding scrambled siRNA (C) were set as control. Images show endocytosed dyes (red) after treatment with Sema3A. Scale bar, 10 μm. (**B** and **D**) Quantification for the uptake of dextran (B) or FM4-64 (D). The ratio between the intensity of dyes and GFP represents endocytosis activity. Data are means ± SEM of three experiments, normalized to control group. **P* < 0.05, ***P* < 0.01, ****P* < 0.001, two-way ANOVA with Bonferroni correction post hoc test.

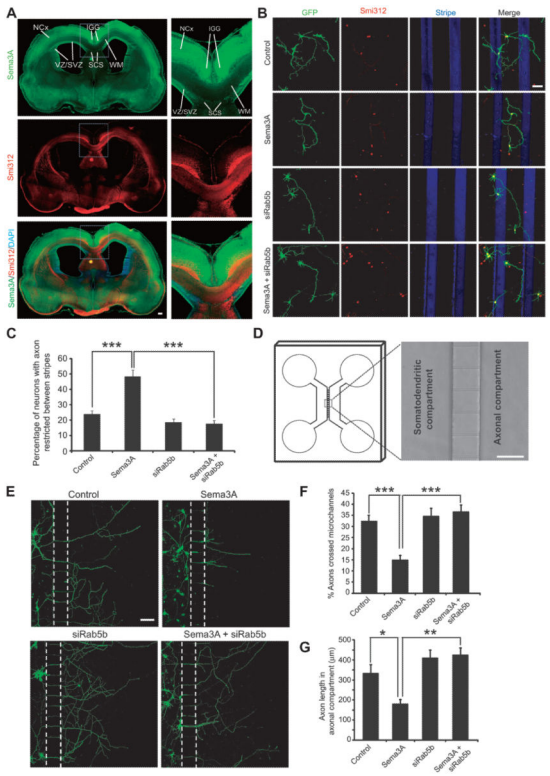

Fig. 5. Sema3A repels and inhibits axonal growth through Rab5

(**A**) E17.5 rat brain slices stained for Sema3A and Smi312, and with DAPI (4′,6-diamidino-2-phenylindole). NCx, neocortex; WM, white matter; VZ/SVZ, ventricular zone/subventricular zone; SCS, subcallosal sling; IGG, indusium griseum glia. Scale bar, 500 μm. (**B** and **C**) Axon patterns of DIV3 L2/3 neurons transfected with Rab5b siRNA (#503) or scrambled siRNA (control) on stripes of Sema3A or control proteins. Images are representatives of at least 127 neurons in each group (B). Data are means ± SEM of three experiments for the percentage of neurons with cell body and axon restricted in the same gap between two stripes. ***$P < 0.001$, two-way ANOVA with Bonferroni correction post hoc test. Scale bar, 60 μm. (**D**) Illustration of two-compartment microfluidic culture system, with magnified area showing microchannels between two compartments. (**E** to **G**) Axonal growth of L2/3 neurons transfected with Rab5b siRNA (#503) or scrambled siRNA into distal compartments without or with the presence of Sema3A (300 ng/ml) added at DIV4. Shown are representatives 48 hours after Sema3A application (E), percentage of axons that had crossed the channels (F), and average length of axons in distal compartment (G). Data are means ± SEM of three experiments. *$P < 0.05$, **$P < 0.01$, ***$P < 0.001$, two-way ANOVA with Bonferroni correction post hoc test. Scale bar, 100 μm.

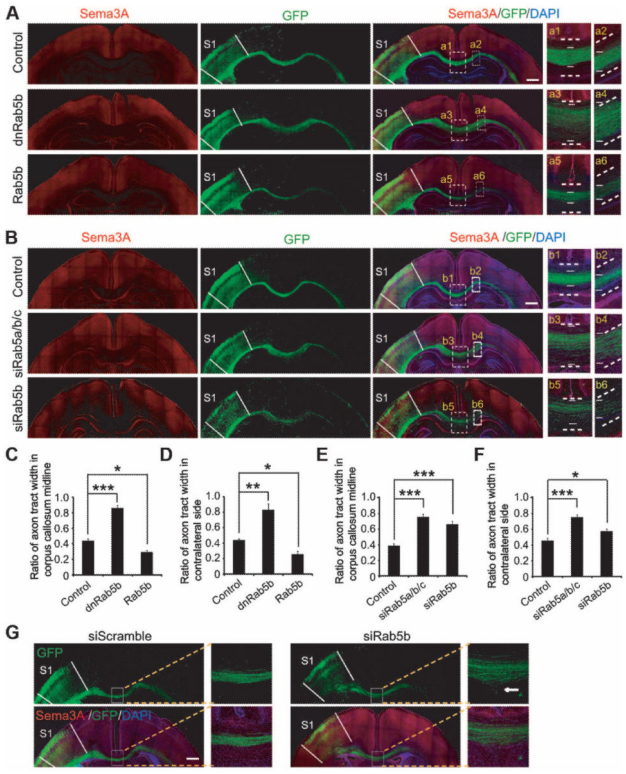

Fig. 6. Rab5 is essential for axon fasciculation in vivo

(**A** and **B**) Callosal axonal patterns of primary somatosensory cortex (S1) and secondary somatosensory cortex (S2) from P7 rats electroporated at E15.5 with indicated plasmids (dnRab5b or Rab5b, siRab5b#503 or siRab5b#503 plus siRab5a#2 and siRab5c#2; Fig. S7, A to C, shows specificity and efficiency of each) together with pCAG-IRES-EGFP, with DAPI indicating cortical layers and corpus callosum landmarks. Boxed areas show axonal tracts in the midline and contralateral side, 1400 μm away from the midline, with dashed white lines marking dorsal-ventral (DV) surfaces of the white matter and short white lines indicating borders of electroporated axonal bundles. Scale bar, 1000 μm. (**C** to **F**) Quantification of the ratio between width of electroporated axonal tracts and that of the entire white matter in the midline (C and E) or contralateral side (D and F) in each group, normalized with GFP intensity in electroporated S1 and S2 regions and that from control group set as 1. Data are means ± SEM from at least three rats in each group. **P* < 0.05, ***P* < 0.01, ****P* < 0.001, one-way ANOVA with Tukey HSD post hoc test. (**G**) Representative images for the effect of decreased Rab5b on callosal axons. Arrow indicates the invasion of axons into the ventral parenchyma underneath the corpus callosum. Scale bar, 1000 μm.

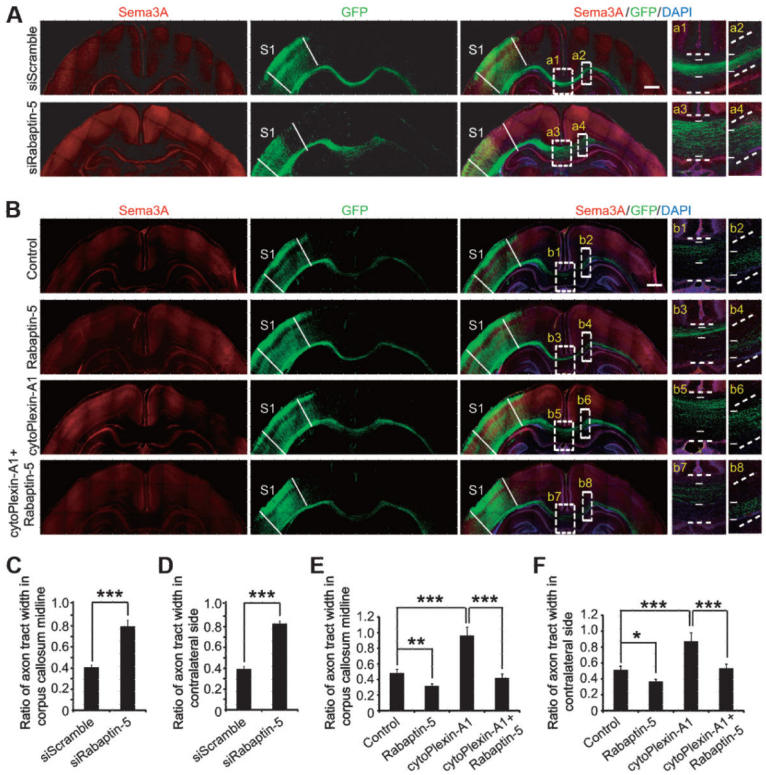

Fig. 7. Role of Rabaptin-5 in axon fasciculation in vivo

(**A** and **B**) Callosal axonal patterns of S1 and S2 from P7 rats electroporated at E15.5 with indicated plasmids and pCAG-IRES-EGFP, with DAPI indicating cortical layers and corpus callosum landmarks. Borders of axonal tracts and the white matter are indicated by short and dashed white lines, respectively. Scale bar, 1000 μm. (**C** to **F**) Quantification for the ratio between the width of electroporated axonal bundles and that of the white matter in the midline (C and E) and contralateral side (D and F) of each group, normalized with GFP intensity in S1 and S2 regions. Data are means ± SEM from at least three rats in each group. $*P < 0.05$, $**P < 0.01$, $***P < 0.001$, one-way ANOVA with Tukey HSD post hoc test (C and D) and two-way ANOVA with Bonferroni correction post hoc test (E and F).

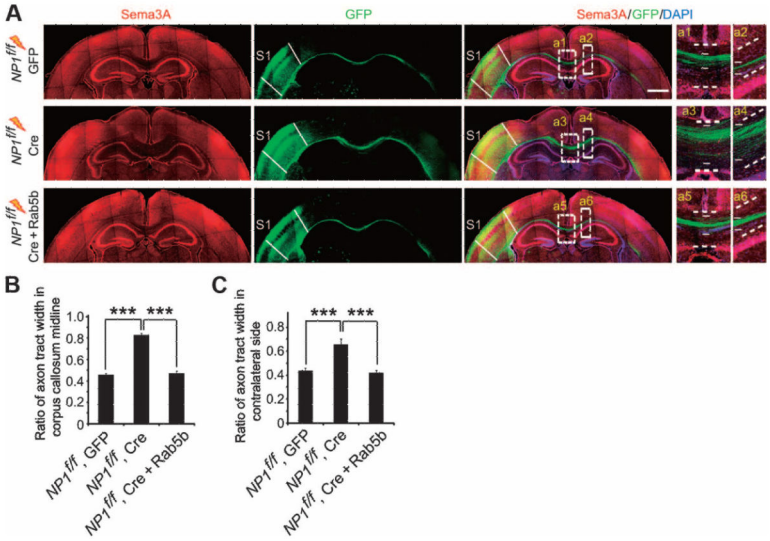

Fig. 8. Rab5 prevents axon defasciculation caused by NP1 knockout

(**A**) E15.5 *NP1*$^{f/f}$ mouse embryos were electroporated with vehicle vector, ubiqutin-Cre-2A-GFP, or ubiqutin-Cre-2A-GFP plus Rab5b, together with pCAG-IRES-EGFP. Callosal axons were analyzed at P7, with DAPI and Sema3A signals revealing the corpus callosum landmarks. Boxed areas show axonal tracts in the midline (a1, a3, a5) and contralateral side (a2, a4, a6), with short and dashed white lines indicating boundaries of electroporated axonal tracts and the white matter, respectively. Scale bar, 1000 μm. (**B** and **C**) Quantification for the ratio between the width of electroporated axonal tracts and that of the white matter in the corpus callosum midline (B) and contralateral side (C) in each group, normalized with GFP intensity in S1 and S2 regions. Data are means ± SEM of at least three mice in each group. ***$P < 0.001$, two-way ANOVA with Bonferroni correction post hoc test.

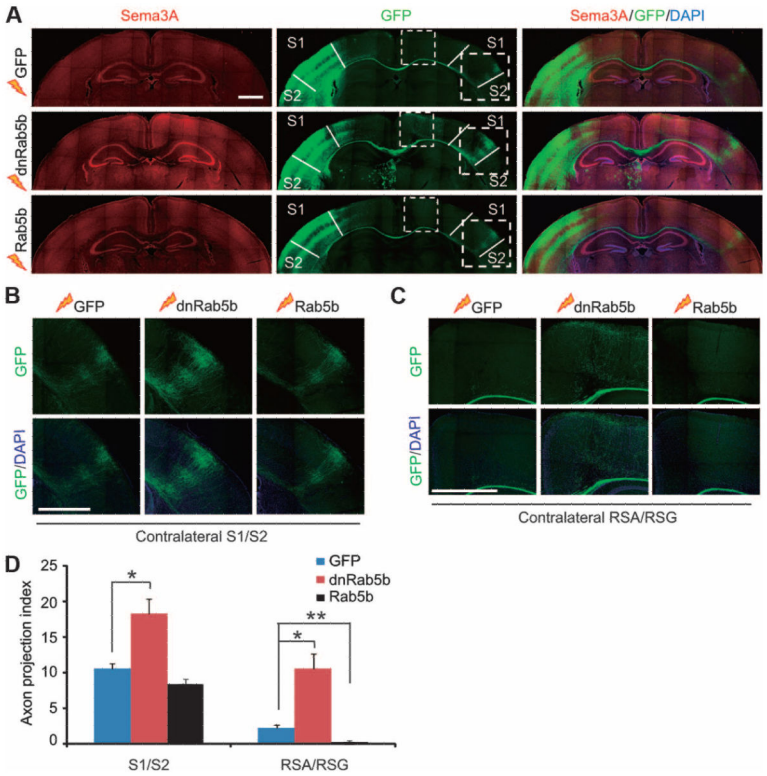

Fig. 9. Inhibition of Rab5 causes mistargeting of contralateral callosal axon trajectories

(**A** to **C**) E15.5 mouse embryos were electroporated with vehicle, Rab5b, or dnRab5b plasmid, together with pCAG-IRES-EGFP. P14 mouse brains at the approximate level of bregma −1.58 mm were coronally sectioned and stained for Sema3A and DAPI to mark cortical layers and the corpus callosum. Boxed areas in (A) indicate contralateral S1 and S2 (B) and RSA and RSG (C) regions, respectively. RSA, retrosplenial agranular cortex; RSG, retrosplenial granular cortex. Scale bars, 1000 μm (A) and 500 μm (B and C). (**D**) Quantification for callosal axon projection index (API), calculated with the following formula: (GFP intensity at indicated region/GFP intensity of total axon bundles in contralateral hemisphere) × 100. Data are means ± SEM from at least four mice in each group. **P* < 0.05, ***P* < 0.01, one-way ANOVA with Tukey HSD post hoc test.

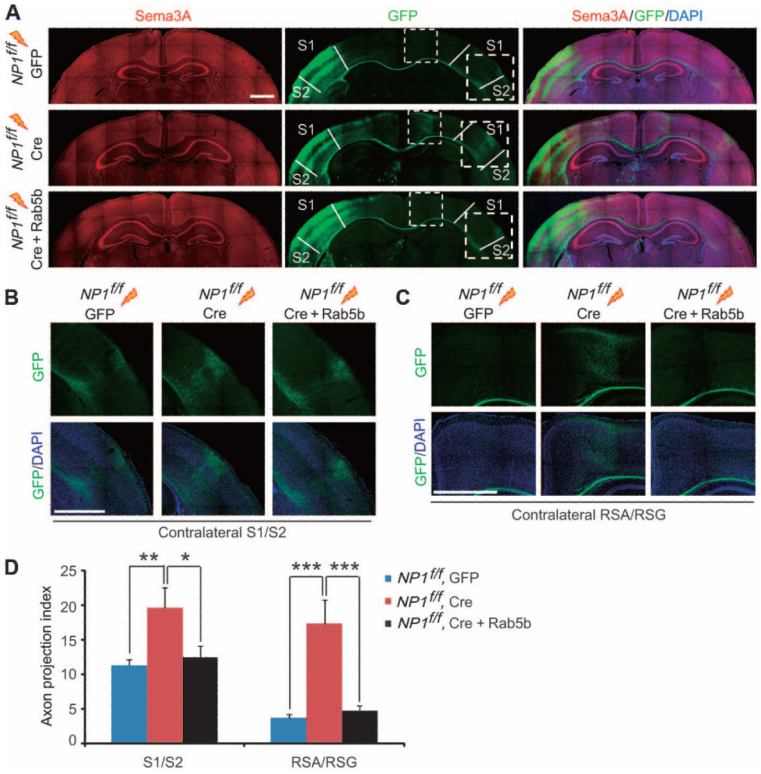

Fig. 10. Forced expression of Rab5 overcomes mistargeting of contralateral axon projections caused by *NP1* knockout

(**A** to **C**) E15.5 *NP1*$^{f/f}$ mouse embryos were electroporated with vehicle vector, ubiqutin-Cre-2A-GFP, or ubiqutin-Cre-2A-GFP plus Rab5b, together with pCAG-IRES-EGFP. P14 mice brains were coronally sectioned and stained for Sema3A and DAPI to mark cortical layers and the corpus callosum. Boxed areas in (A) indicate contralateral S1 and S2 (B) and RSA and RSG (C) regions, respectively. Scale bars, 1000 μm (A) and 500 μm (B and C). (**D**) Quantification for API. Data are means ± SEM from at least three mice in each group. **P* < 0.05, ***P* < 0.01, ****P* < 0.001, two-way ANOVA with Bonferroni correction post hoc test.